

The $D^1\Pi$ state of the NaRb molecule^{*}

O. Docenko¹, M. Tamanis¹, R. Ferber^{1,a}, A. Pashov², H. Knöckel³, and E. Tiemann³

¹ Department of Physics and Institute of Atomic Physics and Spectroscopy, University of Latvia, Rainis Boulevard 19, 1586 Riga, Latvia

² Department of Physics, Sofia University, James Bourchier blvd 5, 1164 Sofia, Bulgaria

³ Institut für Quantenoptik, Universität Hannover, Welfengarten 1, 30167 Hannover, Germany

Received 12 May 2005 / Received in final form 18 July 2005

Published online 17 August 2005 – © EDP Sciences, Società Italiana di Fisica, Springer-Verlag 2005

Abstract. We present a detailed experimental study of the $D^1\Pi$ state of the NaRb molecule by means of Fourier transform spectroscopy of laser induced fluorescence. The entire data field for the $D^1\Pi$ state of Na^{85}Rb and Na^{87}Rb consists of rovibrational levels with $v' = 0\text{--}39$ and $J' = 1\text{--}200$. The data were incorporated into a direct fit of a single potential energy curve to the level energies using the Inverted Perturbation Approach method. The $D^1\Pi$ state q factors, which describe the Λ -doubling, have been obtained in a wide range of rotational and vibrational quantum numbers. Analysis revealed several perturbation regions in the $D^1\Pi$ state.

PACS. 31.50.Df Potential energy surfaces for excited electronic states – 33.20.Kf Visible spectra – 33.50.Dq Fluorescence and phosphorescence spectra

1 Introduction

The renewed interest to the Na+Rb atomic pairs as a candidate for cold collision studies [1] and formation of two-species Bose-Einstein condensate [2] has initiated detailed experimental investigations of the ground $X^1\Sigma^+$ state of the NaRb molecule in a wide range of internuclear distances [3,4]. In reference [4] the $D^1\Pi - X^1\Sigma^+$, $C^1\Sigma^+ - X^1\Sigma^+$ and $B^1\Pi - X^1\Sigma^+$ laser induced fluorescence (LIF) transitions were studied by Fourier transform spectroscopy (FTS) leading to an accurate ground state potential and providing rich spectroscopic information on the upper excited electronic states, particularly on the $D^1\Pi$ state. We present here the $D^1\Pi$ state analysis based on these data.

Up to now spectroscopic information on the $D^1\Pi$ state dissociating to the $\text{Na}(3p_{3/2}) + \text{Rb}(5s_{1/2})$ atomic asymptote is limited. Molecular constants for the bottom of the potential were estimated for the first time in reference [5] from transition frequencies in the D–X LIF spectra as well as their intensity distributions. A few rovibronic levels of the $D^1\Pi$ state with vibrational quantum numbers $v' = 0\text{--}13$ and rotational quantum numbers between $J' = 11$ and 100 were studied. A similar approach was applied in reference [6] where experimental D–X LIF intensities and rovibronic term values were simultaneously

embedded in a non-linear least-square fitting procedure to refine the $D^1\Pi$ potential. Both cited works [5,6] incorporate only a few v' , J' levels measured with relatively low accuracy.

Accurate measurements of the Λ -splitting energy $\Delta_{e/f}$ of particular rovibronic levels of the $D^1\Pi$ state by means of the Radio Frequency – Optical Double Resonance (RF-ODR) method were performed in reference [7]. The measured $\Delta_{e/f}$ values were used to determine the permanent electric dipole moment, which is of the order of 6 D ($2.54\text{D} = 1 ea_0$), for a number of v' , J' levels employing dc Stark effect studies in the $D^1\Pi$ state [7]. Recently the spontaneous lifetimes (about 20 ns) have been determined for a number of $D^1\Pi$ v' , J' levels from LIF decay after pulsed excitation [8].

On the theoretical side two papers are especially important for our study. The most comprehensive theoretical studies of the NaRb molecule have been reported in reference [9] where potential energy curves (PEC) for the ground and several excited states, including the $D^1\Pi$ state, up to their atomic asymptotes are given (see Fig. 1). Note that the PEC's in reference [9] are calculated without spin-orbit effects which cause the 17.196 cm^{-1} fine-structure splitting between the $\text{Na}(3p_{3/2})$ and $\text{Na}(3p_{1/2})$ levels [10]. In reference [6] ab initio calculations of the 11 lowest electronic states potential energy curves, transition dipole moments for a number of electronic transitions, and L -uncoupling matrix elements between $^1\Pi$ and $^1\Sigma^+$ states with respective Λ -doubling constants are presented.

^{*} Supplementary tables (Tabs. I–V) are only available in electronic form at <http://www.eurphysj.org>

^a e-mail: ferber@latnet.lv

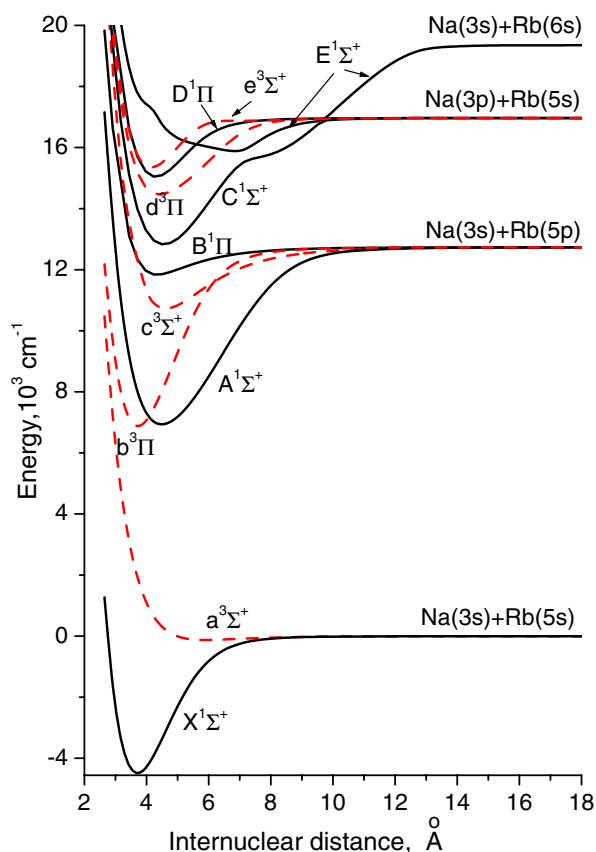


Fig. 1. Potential energy curves for the low lying singlet (solid lines) and triplet (dashed lines) states of NaRb from ab initio calculations [9].

In this paper we report a new study of the $D^1\Pi$ state providing abundant and precise spectroscopic data. Apart from the description of the obtained term energies by means of molecular constants and a potential energy curve, detailed analysis of the observed Λ -doubling for various rovibrational levels is presented.

2 Experiment

Laser induced fluorescence spectra of NaRb were recorded using a Bruker IFS 120 HR Fourier transform spectrometer with a typical resolution of 0.03 cm^{-1} . The experimental set-up has been described in more detail in reference [4]. Briefly, the NaRb molecules were produced in a single section heat-pipe oven similar to that in reference [11] by heating 5 g of Na (purity 99.95%) and 10 g of Rb (purity 99.75 %, natural isotopic composition of ca. 72% ^{85}Rb and 28% ^{87}Rb) from Alfa Aesar. The oven was operated at temperatures between 560 K and 600 K and typically with 2 mbar of Ar as buffer gas. At these conditions apart from the atomic vapour all three types of molecules were formed — Na_2 , Rb_2 and NaRb. The mixture was illuminated by an Ar^+ ion laser or by a frequency doubled Nd:YAG laser.

The Ar^+ ion laser was operated either in a single-mode (typical power 100–500 mW) or in a multimode

(typical power 0.5–3 W) regime. The 514.5 nm, 501.7 nm, 496.5 nm, 488.0 nm, and 476.5 nm laser lines efficiently induced the D–X fluorescence in NaRb. Overall 130 progressions were assigned. The range of vibrational quantum numbers v' observed in the $D^1\Pi$ state with the Ar^+ laser lines is $v' = 0\text{--}39$.

A tunable single mode, frequency doubled Nd:YAG laser with a typical output power of 70 mW at 532.2 nm was also used to excite $D^1\Pi - X^1\Sigma^+$ transitions in NaRb. The laser frequency was varied between 18787.25 cm^{-1} and 18788.44 cm^{-1} giving rise to 38 D–X progressions. The range of vibrational levels excited in the $D^1\Pi$ state by the Nd:YAG laser is $v' = 0\text{--}16$. A list of the NaRb D–X LIF progressions, excited by Ar^+ and Nd:YAG lasers can be found in Table I in the supplementary *Online Material*.

Due to the presence of the argon buffer gas and the very good signal-to-noise ratio some strong fluorescence lines were accompanied by a large number of collisionally induced satellites with ΔJ up to ± 30 . For enriching the rotational relaxation spectra some recordings were made at 10 mbar buffer gas pressure. In a few spectra collisionally induced transitions from the neighbouring vibrational levels were also observed. The analysis of rotational satellites has enlarged the data set of the $D^1\Pi$ state significantly.

As has been already discussed, e.g. in reference [11], by exciting the molecular sample with a single mode laser and by observing the fluorescence in a direction parallel to the laser beam, the resulting fluorescence does not suffer from Doppler broadening. The line frequencies, however, can be shifted from the Doppler-free values within the Doppler profile. As a result, the overall uncertainty of determining the absolute term value from the transition frequencies is generally limited by the Doppler broadening (about 0.03 cm^{-1} FWHM for the typical working temperatures). On the other hand, in the present experiment most of the information on the $D^1\Pi$ state comes from strong lines with abundant rotational satellites. Such strong lines are unlikely to be excited at large detuning from the centre of the parent line. Therefore we initially adopted the experimental uncertainty value of 0.01 cm^{-1} which was later justified by our data analysis.

3 Data analysis

3.1 Term values

The assignment of the excited $D^1\Pi$ state levels for the observed LIF progressions was made in two steps. First, a rotational and isotopic assignment was established by using the $X^1\Sigma^+$ state PEC [4]. Then the energy of the excited level was obtained by adding the experimental transition frequencies to the respective ground state term values calculated with the PEC. The vibrational numbering for $v' \leq 12$ was obtained with the help of the $D^1\Pi$ state Dunham constants and corresponding RKR potential from reference [6]. For higher levels a graphical analysis of the term energies as a function of $J'(J'+1) - 1$ helped us to unambiguously establish the continuation

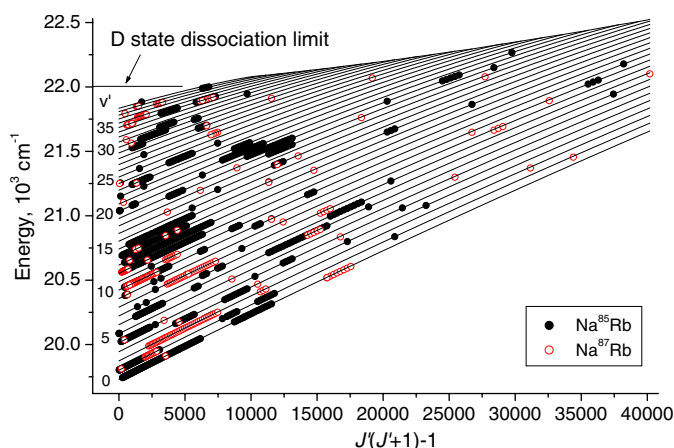


Fig. 2. Plot of the $D^1\Pi$ state experimental term energies against $J'(J'+1)-1$. Solid lines show the calculated term energies, obtained with the IPA potential from Table 2.

of the vibrational numbering. Such plot giving also an overview of the data field is shown in Figure 2.

Overall from the analysis of the Fourier spectra we obtained 1182 term values of Na^{85}Rb and 314 term values of Na^{87}Rb for the $D^1\Pi$ state. The range of vibrational and rotational quantum numbers is $v' = 0-39$ and $J' = 1-200$ respectively. A full list of the experimentally derived term values is given in Table II in the supplementary *Online Material*.

3.2 Λ -doubling and q factors

The $D^1\Pi - X^1\Sigma^+$ rotational relaxation spectra appeared due to collisional populating of neighbouring rotational levels in the $D^1\Pi$ state preferably with the same symmetry (e or f) and subsequent D–X emission according to selection rules for electric dipole transitions. Q lines were typically accompanied by Q satellites, whereas the doublet lines were accompanied by P , R doublet satellites. However, in a number of cases the strongest parent lines had additional satellites coming from the neighbouring rotational levels of the opposite symmetry. Thus, a strong Q line had not only a Q satellite branch, but also the P and R satellites (see Fig. 3). This opened the opportunity to establish directly the Λ -splitting of rotational levels of the $D^1\Pi$ state. From the analysis of the Q lines we obtained f level energies, whereas from the analysis of the P and R lines we obtained the energies of e levels. Then the evaluation of q factors is straightforward:

$$E_e - E_f = \Delta_{e/f} = qJ'(J'+1). \quad (1)$$

This allowed us to obtain q factor values and their sign for 20 vibrational levels in the interval $v' = 0-35$ in a wide range of rotational quantum numbers ($J' = 20-122$).

For most of the vibrational levels q factors are around $0.9 \times 10^{-5} \text{ cm}^{-1}$. As q factors are calculated from the Λ -splitting energy $\Delta_{e/f}$ (1), q factor uncertainty is determined by the uncertainty of the Λ -splitting energy of about 0.004 cm^{-1} . The latter arises mainly from two

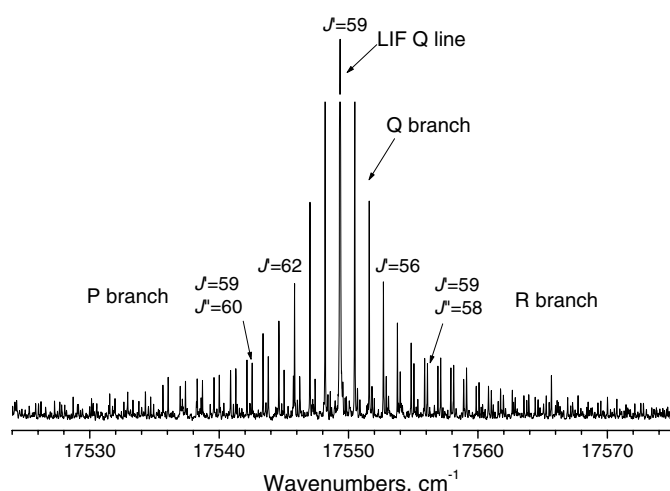


Fig. 3. P , Q , R collisionally induced rotational satellites accompanying the parent Q transition ($D^1\Pi(13, 59) \rightarrow X^1\Sigma^+(30, 59)$) excited with the Ar^+ laser line 488.0 nm .

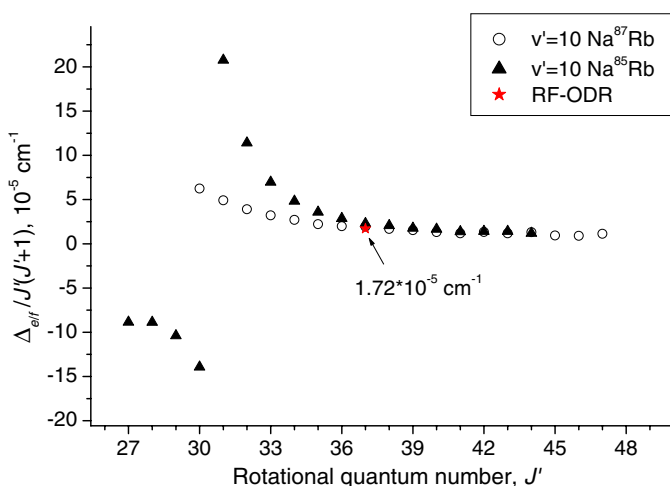


Fig. 4. The dependence of $\Delta_{e/f}/J'(J'+1)$ on J' for $v' = 10$ level in Na^{85}Rb (triangles) and Na^{87}Rb (open circles). The arrow marks the q factor determined from the RF-ODR experiment, see Table 1.

sources: the uncertainty of the experimental D–X transition energy difference (0.003 cm^{-1}) and the uncertainty of the calculated energy difference between the ground state levels (0.003 cm^{-1} , as stated in Ref. [4]). Note, that the q factor uncertainty scales with $1/J'(J'+1)$.

In few cases an anomalous behaviour of the Λ -splittings was observed, clearly indicating a local perturbation in the $D^1\Pi$ state. Figure 4 presents an example of such a perturbation for the vibrational level $v' = 10$ with the perturbation center around $J' = 31$ for Na^{85}Rb .

Analysis of q factors outside the local perturbation regions in $v' = 0-30$ range did not reveal a vibrational or isotopomer dependence within our accuracy, whereas a slight decrease of q factors with J' was observed. Thus it was possible to describe the whole set of q factors by one J' -dependence

$$q = q_0 + q_1 J'. \quad (2)$$

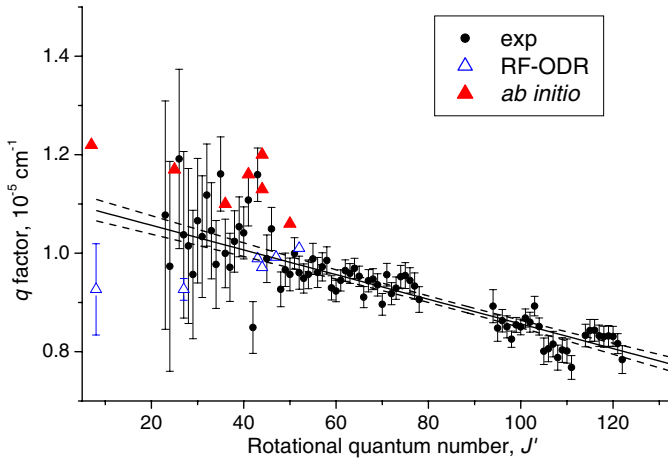


Fig. 5. $D^1\Pi$ state unperturbed q factors (circles), averaged for different vibrational levels and isotopomers. The solid line corresponds to the fitted linear dependence $\bar{q} = [1.079 - 0.00230J']10^{-5} \text{ cm}^{-1}$ and the dashed lines denote the 95% confidential region. Full triangles are *ab initio* q factors from reference [6]. Open triangles are RF-ODR q factor values (see Tab. 1).

Figure 5 presents ca. eighty q factors plotted as a function of J' . These q values are obtained from about 1000 experimental q factors after a weighted average for a given J' . The large scatter of q values for low J' comes from the very small Λ -splittings, which are comparable with the experimental uncertainty. The resulting fit parameters in (2) are $q_0 = 1.079(14) \times 10^{-5} \text{ cm}^{-1}$ and $q_1 = -2.30(15) \times 10^{-8} \text{ cm}^{-1}$. A list of the experimentally derived q factors is given in Table III in the supplementary *Online Material*.

The q factors measured in this work are consistent with the RF-ODR measurements [6], which are of higher accuracy, but cover a very limited set of measured levels with $J' \leq 52$. The values $q_{\text{RF-ODR}}$ presented in Table 1 and Figure 5 have been recalculated using experimental Λ -splitting values from reference [7] and the recently established correct J' assignment from reference [4].

A comparison between the experimental q factors and the *ab initio* calculations from reference [6] is included in Table 1 and Figure 5. The *ab initio* q factors were obtained from the electronic structure calculations performed by means of the many-body multipartitioning perturbation theory (MPPT), using the singlet-singlet approximation, i.e. the Λ -splitting is determined by electronic-rotational perturbations caused by distant singlet $^1\Sigma^+$ states. Analysis of L -uncoupling matrix elements between the $D^1\Pi$ state and the X, A, C and $E^1\Sigma^+$ states showed that the Λ -splitting in the $D^1\Pi$ state is mainly determined by the interaction with the $C^1\Sigma^+$ state. The calculated q factors are in good agreement with the experimental data, but slightly larger (see Fig. 5), probably because of neglecting the influence of the $^1\Sigma^+$ states higher than the $E^1\Sigma^+$ state in the calculations.

Note that the only experimental q factor in Table 1 showing strong deviation from calculations is the one for

Table 1. The $D^1\Pi$ state $q_{\text{RF-ODR}}$ factors (in 10^{-5} cm^{-1}) obtained from the RF-ODR experiments in reference [7] and recalculated for correct J' values; J' in parentheses corresponds to the previous assignment from reference [7]. The given uncertainty is one standard deviation. $q_{\text{ab initio}}$ are the calculated values from reference [6].

Isotopomer	v'	$J'(J'[7])$	$q_{\text{RF-ODR}}$	$q_{\text{ab initio}}$
Na ⁸⁵ Rb	0	44(44)	0.971 ± 0.003	+1.20
Na ⁸⁵ Rb	1	8(7)	0.93 ± 0.09	+1.22
Na ⁸⁵ Rb	4	27(25)	0.93 ± 0.02	+1.17
Na ⁸⁵ Rb	4	43(41)	0.989 ± 0.002	+1.16
Na ⁸⁵ Rb*	6	47(44)	0.992 ± 0.003	+1.13
Na ⁸⁷ Rb	10	37(36)**	1.723 ± 0.002	+1.10
Na ⁸⁵ Rb	12	52(50)	1.0101 ± 0.0012	+1.06

* Isotopomer changed compared to reference [7]

** Perturbed level

the level $v' = 10$, $J' = 37$. Present measurements (see Fig. 4) support the statement already proposed in reference [6] that this discrepancy is attributed to a local perturbation.

3.3 Construction of PEC

The $D^1\Pi$ state for both isotopomers of NaRb is described in the adiabatic approximation with a single potential energy curve. The potential was defined as proposed in reference [12] as a set of points $\{R_i, U(R_i)\}$ connected by cubic spline functions. The values of the potential $U(R_i)$ were adjusted in an iterative procedure which searches for best agreement between the experimentally observed and calculated term values. In order to avoid unphysical oscillations in the regions not sufficiently determined by the experimental data, we applied the regularization procedure recently suggested in reference [13].

As initial guess for the potential curve we took the RKR potential constructed using molecular constants from reference [6]. Since the shift of the f levels under the influence of higher Σ^- states is expected to be very small, the potential fit was based on the f levels considered as “unshifted”. The e levels were also included in the fit after subtracting from their experimental term energies the value of the Λ -splitting $q(J')J'(J'+1)$ determined in the previous section. Levels showing deviations more than 0.03 cm^{-1} (7% of the whole data set) were not included in the final fitting procedure, these levels are considered either as perturbed (see Sect. 3.4 below) or as Doppler shifted levels. Taking into account the $q(J')$ dependence of equation (2), the final potential fits all unperturbed energy levels of both isotopomers with a standard deviation of 0.008 cm^{-1} and a dimensionless standard deviation of 0.78. It consists of 35 points and is given in Table 2. In order to interpolate the potential, a natural cubic spline [14] through all 35 grid points should be used. Note, that if the J' dependence of the q factors is neglected and a single averaged q factor ($0.87 \times 10^{-5} \text{ cm}^{-1}$) is used, we get a standard deviation of 0.009 cm^{-1} and a dimensionless standard deviation of 0.88.

Table 2. List of the grid points of the potential energy for the NaRb D¹Π state. Energies are given with respect to the minimum of the ground state [4].

R (Å)	$U(R)$ (cm ⁻¹)	R (Å)	$U(R)$ (cm ⁻¹)
2.80000	26088.574	5.28571	20599.728
2.97500	23892.559	5.42857	20762.635
3.15000	22416.175	5.57143	20916.356
3.32500	21452.447	5.71429	21058.223
3.50000	20753.769	5.85714	21186.491
3.60000	20448.239	6.00000	21300.660
3.70000	20203.231	6.29429	21491.459
3.80000	20013.336	6.58857	21630.673
3.90000	19872.445	6.88286	21729.052
4.00000	19775.498	7.17714	21798.073
4.14286	19703.369	7.64762	21870.204
4.28571	19697.224	8.11810	21915.936
4.42857	19744.947	8.58857	21945.594
4.57143	19835.458	9.05905	21964.683
4.71429	19958.393	9.52952	21977.465
4.85714	20104.327	9.86476	21984.053
5.00000	20264.751	10.20000	21989.488
5.14286	20432.036		

$R_{\text{out}} = 9.94559 \text{ \AA}$	$D = 22003.868 \text{ cm}^{-1}$
$C_6 = -1.5046 \times 10^7 \text{ cm}^{-1} \text{ \AA}^6$	
$C_8 = 3.4178 \times 10^9 \text{ cm}^{-1} \text{ \AA}^8$	
$C_{10} = -1.6265 \times 10^{10} \text{ cm}^{-1} \text{ \AA}^{10}$	

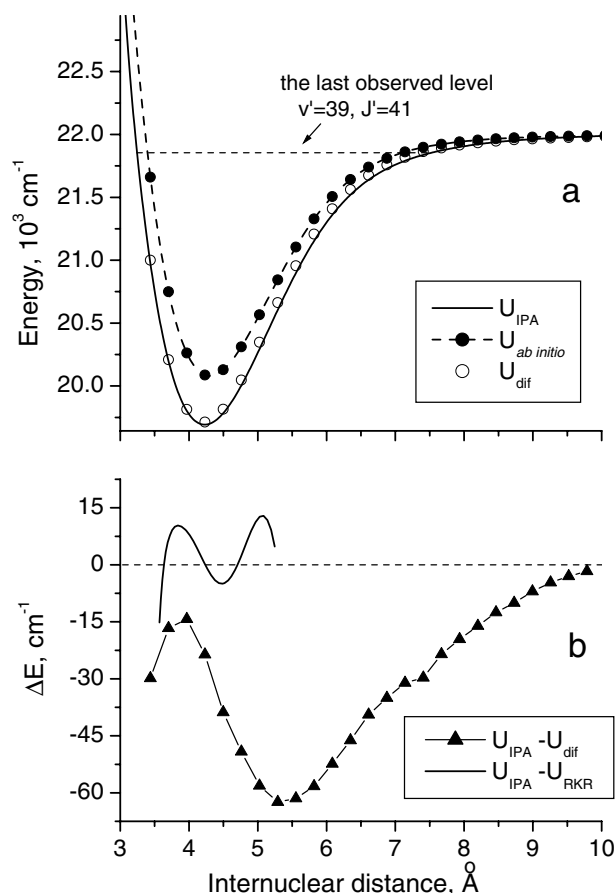
Potential minimum	
$R_m = 4.2279 \text{ \AA}$	$T_m = 19692.564 \text{ cm}^{-1}$

Initially, the PEC was constructed in a pointwise form up to 10 Å. In order to ensure the proper asymptotic behaviour of the potential we connected the PEC with a long-range (LR) branch, for which we adopted the usual dispersion form

$$U(R) = D - C_6 R^{-6} - C_8 R^{-8} - C_{10} R^{-10} \quad (3)$$

with coefficients C_6 and C_8 taken from reference [15]. The dissociation asymptote D of the D¹Π state correlating to the Na(3p_{3/2}) + Rb(5s_{1/2}) atomic limit was calculated from the Na(3p_{3/2}) level energy [10] (neglecting hyperfine structure, referred to the hyperfine center of gravity) and the X¹Σ⁺ state dissociation energy. We used the ground state dissociation energy value 5030.50(10) cm⁻¹ which differs from the published one [4], because it is the result of a new combined evaluation of the X¹Σ⁺ and a³Σ⁺ states which will be published elsewhere [16]. The connecting point R_{out} and the C_{10} parameter were varied in order to ensure a smooth connection with the pointwise potential. Thus, the C_{10} parameter presented here should be considered as an effective coefficient.

In Figure 6a the experimental IPA potential is compared with the ab initio potential from reference [9] (full circles). Also the difference based potential $U(D)_{\text{dif}} = U(X)_{\text{exp}} + (U(D)_{\text{ab initio}} - U(X)_{\text{ab initio}})$ suggested in references [6,17] as an improved estimate from ab initio results is given in Figure 6a (open circles). It is produced

**Fig. 6.** (a) Comparison of the new determination of the D¹Π state IPA potential (solid line) with the corresponding ab initio potential by Korek et al. [9] (full circles) and the difference based potential (open circles), moved to the correct atomic limit. (b) Difference of the IPA potential U_{IPA} with respect to the difference based potential (triangles) and to the RKR potential U_{RKR} from reference [6] (solid line).

from the difference of the ab initio D¹Π and X¹Σ⁺ state potentials given in reference [9], which is then added to the experimental ground state potential $U(X)_{\text{exp}}$ given in reference [4]. As can be seen, the difference based potential is much closer to the IPA potential than the ab initio one. Similar conclusions are obtained in references [17,18], in which the A¹Σ⁺–b³Π complex and the C¹Σ⁺ state of the NaRb molecule were studied. The difference between the IPA potential and the RKR potential from reference [6] is shown in Figure 6b.

For the convenience of simple spectroscopic estimations we have also fitted a Dunham expansion with the conventional Y_{lk} coefficients to the unperturbed energy levels, where, l , k are powers of $(v' + 1/2)$ and $[J'(J' + 1) - 1]$, respectively. The levels are described with a standard deviation of 0.009 cm⁻¹ and a dimensionless standard deviation of 0.87 for both isotopomers. The Dunham parameters, rounded as described in reference [19], are listed in Table 3. It is worth mentioning that the $T_e = 19692.06 \text{ cm}^{-1}$, $R_e = 4.2155 \text{ \AA}$, $\omega_e = 73.26 \text{ cm}^{-1}$ and $B_e = 0.05244 \text{ cm}^{-1}$ values from reference [6] for

Table 3. Dunham parameters (in cm^{-1}) of the Na^{85}Rb $D^1\Pi$ state for $v' \leq 39$, $J' \leq 200$, valid also for Na^{87}Rb employing the conventional mass relations.

T_e	19692.5496
$Y(0,0)$	-0.019
$Y(1,0)$	73.10306
$Y(2,0)$	-0.281142
$Y(3,0)$	-0.53893 $\times 10^{-2}$
$Y(4,0)$	0.11707 $\times 10^{-3}$
$Y(6,0)$	-0.40941 $\times 10^{-6}$
$Y(7,0)$	0.18988 $\times 10^{-7}$
$Y(8,0)$	-0.3688 $\times 10^{-9}$
$Y(9,0)$	0.27 $\times 10^{-11}$
$Y(0,1)$	0.5212303 $\times 10^{-1}$
$Y(1,1)$	-0.221455 $\times 10^{-3}$
$Y(2,1)$	-0.62437 $\times 10^{-5}$
$Y(3,1)$	0.33948 $\times 10^{-6}$
$Y(4,1)$	-0.30585 $\times 10^{-7}$
$Y(5,1)$	0.1196 $\times 10^{-8}$
$Y(6,1)$	-0.252 $\times 10^{-10}$
$Y(7,1)$	0.20 $\times 10^{-12}$
$Y(0,2)$	-0.105723 $\times 10^{-6}$
$Y(1,2)$	-0.12890 $\times 10^{-8}$
$Y(2,2)$	0.202 $\times 10^{-10}$
$Y(3,2)$	-0.473 $\times 10^{-11}$
$Y(5,2)$	0.423 $\times 10^{-14}$
$Y(6,2)$	-0.104 $\times 10^{-15}$
$Y(0,3)$	0.2124 $\times 10^{-12}$
$Y(3,3)$	-0.1245 $\times 10^{-15}$
$Y(4,3)$	0.1342 $\times 10^{-16}$
$Y(5,3)$	-0.345 $\times 10^{-18}$
$Y(0,4)$	-0.118 $\times 10^{-17}$
$Y(1,4)$	-0.141 $\times 10^{-18}$
$Y(4,4)$	-0.95 $\times 10^{-22}$

Na^{85}Rb are rather close to the ones in the present work. The Dunham parameters and the potential grid points are also given in Table IV in the supplementary *Online Material*.

3.4 Perturbations

As stated above, the obtained PEC fits most of the observed levels with a standard deviation of 0.008 cm^{-1} . However, we have measured a number of v' , J' levels whose experimental term values deviate from the calculated ones by more than 0.03 cm^{-1} indicating a possible presence of local perturbations. In cases where a long series of rotational satellites was observed we could follow how both e and f components behave in the particular local perturbation region. In Figure 7 differences between the observed term values (E_{exp}) and energies calculated with the PEC (E_{calc}) are shown for vibrational levels $v' = 23$ and 10. It is obvious that both e and f components are perturbed in the presented J' ranges.

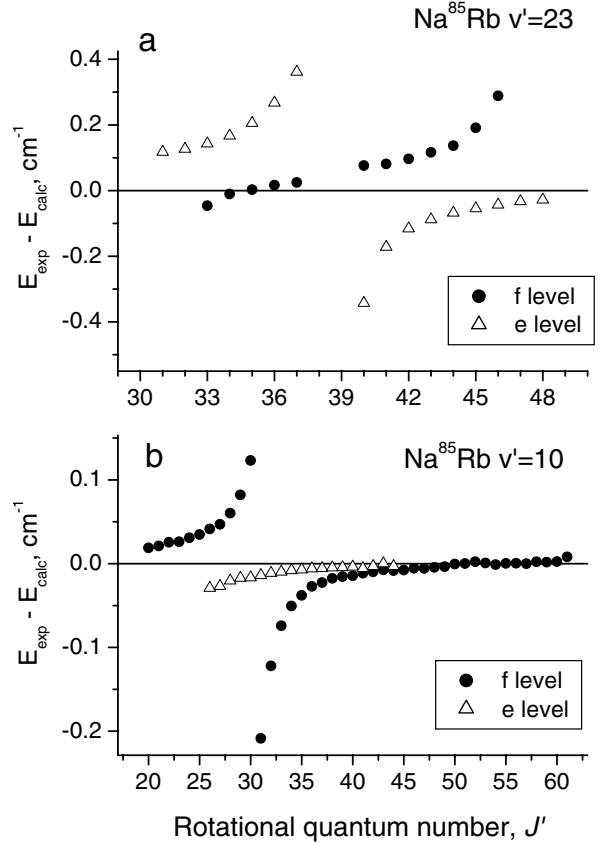


Fig. 7. The difference between observed and unperturbed (calculated from the IPA potential) term energies for vibrational levels $v' = 23$ (a) and $v' = 10$ (b) of the $D^1\Pi$ state.

This means that perturbations are caused by nearby triplet states, apparently the $d^3\Pi$ or the $e^3\Sigma^+$, see Figure 1. For higher vibrational levels the additional influence of the $E^1\Sigma^+$ state cannot be excluded.

We have to confess that we were not able to study perturbations systematically due to the accidental character of optical excitations of different v' , J' levels by fixed-frequency laser lines. Nevertheless, we have found more than 10 perturbation regions in the $v' = 0-39$ interval. The largest observed deviation of a term value reached almost 2 cm^{-1} for $v' = 38$, $J'_e = 79$. A list of perturbation regions is given in Table V in the supplementary *Online Material*.

4 Conclusions

In this paper the NaRb $D^1\Pi$ state is studied by laser induced fluorescence Fourier transform spectroscopy. More than 1400 $D^1\Pi$ state level energies with accuracy of 0.01 cm^{-1} were obtained in a wide range of vibrational and rotational quantum numbers.

A pointwise PEC, as well as a Dunham expansion were fitted to the experimental energies of the unperturbed $D^1\Pi$ state levels. The present FTS measurements characterize 93.5% of the $D^1\Pi$ state potential well of the NaRb

molecule. The $D^1\Pi$ state dissociation energy obtained in the present experiment is $2311.30(14) \text{ cm}^{-1}$. The accuracy of the derived $D^1\Pi$ state dissociation energy is associated with the accuracy of the $X^1\Sigma^+$ state dissociation energy [16] and the estimated uncertainty of 0.1 cm^{-1} of the $D^1\Pi$ state potential minimum value. The dissociation energy with respect to the first bound level ($v' = 0$, $J' = 1f$) is $2274.79(10) \text{ cm}^{-1}$.

A large set of q factors in the $D^1\Pi$ state was obtained allowing one to derive their dependence on the rotational quantum number J' . No vibrational dependence of q factors was observed within the accuracy of present measurements. In several cases an anomalous behaviour of a q factor was observed, clearly indicating a local perturbation in the $D^1\Pi$ state.

Analysis of perturbation regions revealed that both e and f components are perturbed, thus testifying to the triplet character of perturbing state. Apparently, either the $d^3\Pi$ or the $e^3\Sigma^+$ state perturbs the $D^1\Pi$ state.

The work is supported by the DFG through SFB 407 and GRK 665. O.D., M.T. and R.F. acknowledge the support by the NATO Sfp 978029 Optical Field Mapping grant and by the EC 5th Frame "Competitive and Sustainable Growth" Grant G1MA-CT-2002-04063, as well as by Latvian Science Council grants No. 04.1308 and Latvian Government Grants ES 03-40 and TOP 04-44. A.P. acknowledges the support from the Alexander von Humboldt Foundation. The authors are indebted to Dr. A.V. Stolyarov, Dr. E.A. Pazyuk and Dr. A. Zaitsevskii for useful discussions.

References

- G.D. Telles, L.G. Marcassa, S.R. Muniz, S.G. Miranda, A. Antunes, C. Westbrook, V.S. Bagnato, *Phys. Rev. A* **59**, R23 (1999)
- S.B. Weiss, M. Bhattacharya, N.P. Bigelow, *Phys. Rev. A* **68**, 042708 (2003)
- O. Docenko, O. Nikolayeva, M. Tamanis, R. Ferber, E.A. Pazyuk, A.V. Stolyarov, *Phys. Rev. A* **66**, 052508 (2002)
- O. Docenko, M. Tamanis, R. Ferber, A. Pashov, H. Knöckel, E. Tiemann, *Phys. Rev. A* **69**, 042503 (2004)
- N. Takahashi, H. Katô, *J. Chem. Phys.* **75**, 4350 (1981)
- A. Zaitsevskii, S.O. Adamson, E.A. Pazyuk, A.V. Stolyarov, O. Nikolayeva, O. Docenko, I. Klincare, M. Auzinsh, M. Tamanis, R. Ferber, R. Cimiraglia, *Phys. Rev. A* **63**, 052504 (2001)
- O. Nikolayeva, I. Klincare, M. Auzinsh, M. Tamanis, R. Ferber, E.A. Pazyuk, A.V. Stolyarov, A. Zaitsevskii, R. Cimiraglia, *J. Chem. Phys.* **113**, 4896 (2000)
- I. Klincare, M. Tamanis, R. Ferber, *Chem. Phys. Lett.* **382**, 593 (2003)
- M. Korek, A.R. Allouche, M. Kobeissi, A. Chaalan, M. Dagher, K. Fakhreddin, M. Aubert-Frecon, *Chem. Phys.* **256**, 1 (2000)
- P. Juncar, J. Pinar, J. Hamon, A. Chartier, *Metrologia* **17**, 77 (1981)
- O. Allard, A. Pashov, H. Knöckel, E. Tiemann, *Phys. Rev. A* **66**, 042503 (2002)
- A. Pashov, W. Jastrzebski, P. Kowalczyk, *Comput. Phys. Commun.* **128**, 622 (2000)
- A. Grochola, W. Jastrzebski, P. Kowalczyk, A. Pashov, *J. Chem. Phys.* **121**, 5754 (2004)
- W.H. Press, S.A. Teukolski, W.T. Vetterling, B.P. Flannery, *Numerical Recipes in Fortran 77* (Cambridge University Press, Cambridge, 1992)
- B. Bussery, Y. Achkar, M. Aubert-Frecon, *Chem. Phys.* **116**, 319 (1987)
- A. Pashov, O. Docenko, M. Tamanis, R. Ferber, H. Knöckel, E. Tiemann, in preparation
- M. Tamanis, R. Ferber, A. Zaitsevskii, E.A. Pazyuk, A.V. Stolyarov, Hongmin Chen, Jiangbing Qi, Henry Wang, W.C. Stwalley, *J. Chem. Phys.* **117**, 7980 (2002)
- W. Jastrzebski, P. Kortyka, P. Kowalczyk, O. Docenko, M. Tamanis, R. Ferber, A. Pashov, H. Knöckel, E. Tiemann, *Eur. Phys. J. D* **36**, 57 (2005)
- R.J. Le Roy, *J. Mol. Spectrosc.* **191**, 223 (1998)